9. Milton GW, Balch CM, Shaw HM, et al. Prophylactic lymph node dissection in clinical stage I cutaneous melanoma: results of surgical treatment in 1319 patients. *Br J Surg* 1982;69:108–113.
10. Wanebo HJ, Woodruff J, Fortner JG, et al. Malignant melanoma of the extremities: a clinicopathological study using level of invasion (microstage). *Cancer* 1975;35:666–673.
11. Sugarbaker EV, McBride CM. Melanoma of the trunk: the results of surgical excision and anatomic guidelines for predicting nodal metastasis. *Surgery* 1976;80:22–30.
12. Veronesi V, Adamus J, Bandiera DC. Delayed regional lymph node dissection in stage I melanoma of the skin of the lower extremities. *Cancer* 1982;49:2420–2430.
13. Bailet JW, Abermayer E, Tabour BA, et al. Positron emission tomography: a new precise imaging modality for detection of primary head and neck tumors and assessment of cervical adenopathy. *Laryngoscope* 1992;102:281–288.
14. Friedman M, Mafee MF, Pacella BL, et al. Rationale for elective neck dissection in 1990. *Laryngoscopy* 1990;110:443–449.
15. Friedman M, Dew LL, Mafee MF, et al. Metastatic neck disease: evaluation by computed tomography. *Arch Otolaryngol* 1984;110:443–446.
16. Hillsamer PJ. Improving diagnostic accuracy of cervical metastases with computed tomography and magnetic resonance imaging. *Arch Otolaryngol Head Neck Surg* 1990;116:1297–1304.
17. Hays, SD, Eremin O. The relevance of tumor draining lymph nodes in cancer. *Surg Gynecol Obstet* 1992;174:533–535.
18. Mancuso AA, Harnsberger HR, Muraki AS, et al. Computed tomography of cervical and retropharyngeal lymph nodes: normal anatomy, variants of normal and applications in staging head and neck cancer, Part II; pathology. *Radiology* 1983;148:715–721.
19. Mancuso AA, Maceri D, Rice D, et al. CT of cervical lymph node cancer. *Am J Radiol* 1981;136:381–384.
20. Shaukat A. False-positive and false negative neck nodes. *Head Neck Surg* 1985;8:78–81.
21. Stern WB, Silver CE, Zeifer BA, et al. Computed tomography of the clinically negative neck. *Head Neck Surg* 1990;12:109–114.
22. Stevens MH, Harnsberger HR, Mancuso AA, et al. Computed tomography of cervical lymph nodes. *Arch Otolaryngol* 1985;111:735–741.
23. Salk D and the Multicenter Study Group. Technetium-labeled monoclonal antibodies for imaging metastatic melanoma: results of a multicenter clinical study. *Semin Oncol* 1988;15:608–618.
24. Blend MJ, Ronan SG, Salk DJ, et al. Role of ^{99m}Tc labeled monoclonal antibody in the management of melanoma patients. *J Clin Oncol* 1992;10:1330–1337.
25. Fritzberg AR, Abrams PG, Beaumier PL, et al. Specific and stable labeling of antibodies with technetium-99m with a diamide dithiolate chelating agent. *Proc Nat Acad Sci USA* 1988;85:4025–4029.
26. Schroff RW, Foon KA, Bealty SM, et al. Human antimurine immunoglobulin responses in patients receiving monoclonal antibody therapy. *Cancer Res* 1985;45:879–885.
27. Kirkwood JM, Myers JE, Vlock DR, et al. Tomographic gallium-67 citrate scanning; useful new surveillance for metastatic melanoma. *Ann Intern Med* 1982;67:694–699.
28. Milder MS, Frankel RS, Bulkley GB, et al. Gallium-67 scintigraphy in malignant melanoma. *Cancer* 1973;32:1350–1356.
29. Romolo JL, Fisher RS. Gallium-67 scanning compared with physical examination in the preoperative staging of malignant melanoma. *Cancer* 1979;44:468–471.
30. Alex JC, Weaver DL, Fairbank JT, et al. Gamma probe-guided lymph node localization in malignant melanoma. *Surg Oncol* 1993;2:303–308.
31. Alex JC, Krag DN. Gamma-probe guided localization of lymph nodes. *Surg Oncol* 1993;2:137–143.
32. Elliott AT, MacKie RM, Murray T, et al. A comparative study of the relative sensitivity and specificity of radiolabeled monoclonal antibody and computerized tomography in the detection of sites of disease in human malignant melanoma. *Br J Cancer* 1989;59:600–604.

Fluorine-18-Fluorodeoxyglucose PET Imaging of Soft-Tissue Sarcoma

Omgo E. Nieweg, Jan Pruim, Robert J. van Ginkel, Harald J. Hoekstra, Anne M.J. Paans, Willemina M. Molenaar, Heimen Schraffordt Koops and Willem Vaalburg

Division of Surgical Oncology, Department of Surgery, Department of Pathology and National PET Research Center, University Hospital Groningen, Groningen, The Netherlands; and Department of Surgery, The Netherlands Cancer Institute, Amsterdam, The Netherlands

PET with ^{18}F-fluoro-2-deoxy-D-glucose (FDG) was used to study soft-tissue lesions. The goals of the study were to establish FDG uptake in soft-tissue sarcoma, to determine the sensitivity of this technique, to investigate the correlation between histologic grade and glucose consumption and to determine whether FDG-PET can discriminate between benign and malignant lesions. **Methods:** PET imaging was performed in 18 patients with soft-tissue sarcoma and 4 patients with a benign soft-tissue lesion. Glucose consumption in the tumors was calculated using Patlak's graphical analysis with an assumption made for the lumped constant. Standardized uptake values also were calculated. **Results:** All soft-tissue sarcomas were clearly depicted. The median glucose consumption was 13.0 μmole/100 g/min (range 2.9–41.8 μmole/100 g/min). A correlation was found between glucose metabolism and the histopathologic malignancy grade. Such a correlation was not demonstrated for the standardized uptake values. One benign lesion was also visualized. Benign lesions were not visualized in two patients and in the remaining patient an equivocal scan was obtained. Benign lesions could be distinguished from high-grade malignant lesions but not consistently from lesions with low or intermediate malignancy grades. **Conclusion:** PET with FDG is an effective technique to visualize soft-tissue sarcomas. We found a sensitivity of 100%. There is a correlation between glucose metabolic rate and tumor malignancy grade. FDG appears to be unsuitable for discriminating benign lesions from soft-tissue sarcomas with low or intermediate malignancy grades.

Key Words: soft-tissue sarcomas; neoplasms; tumor grading; PET

J Nucl Med 1996; 37:257–261

Soft-tissue sarcomas are malignant tumors that can arise from mesenchymal structures at any site in the body. These tumors constitute 1% of all cancers. They often reach a large size before a diagnosis is established. Soft-tissue sarcomas are known to invade surrounding normal tissues and disseminate to distant sites, most often to the lungs. The presence or absence of metastases and the tumor malignancy grade will dictate the therapeutic regimen. The fact that ^{18}F-fluoro-2-deoxy-D-glucose (FDG) is concentrated in various types of tumor tissue (*1*) and the ability of PET to analyze aspects of tumor biology suggest that PET may be of particular value in the therapy of patients with such tumors.

The goals of this study were to establish FDG uptake in soft-tissue sarcoma, to determine sensitivity (percentage of sarcomas that were visualized on the images), to investigate the correlation between histologic grade, regional glucose metabolic rate (RMR_{gl}) and standardized uptake values (SUV), and to determine whether PET with FDG can differentiate between benign and malignant lesions.

Received Dec. 7, 1994; revision accepted Jul. 14, 1995.

For correspondence contact: Omgo E. Nieweg, MD, Department of Surgery, The Netherlands Cancer Institute, Antoni van Leeuwenhoek Huis, Plesmanlaan 121, 1066 CX Amsterdam, The Netherlands.

TABLE 1
Clinical Data

Diagnosis	No.	Size (cm)	Grade I	Grade II	Grade III
Malignant tumors					
Malignant fibrous histiocytoma	6	3.2, 4.5*, 5.0, 11.5, 13.7†	2		3
Liposarcoma	5	7.0, 11.3, 15.0, 20.0, 22.5	1	3	1
Synovial sarcoma	2	7.0, 10.3			2
Extraskeletal chondrosarcoma	1	5.7			1
Rhabdomyosarcoma	1	8.3			1
Fibrosarcoma	1	17.5			1
Sarcoma, not otherwise classified	1	31.0			1
Neuroepithelioma	1	7.0			1
Benign lesions					
Myxoma	1	2.4			
Ganglion	1	4.8			
Lymphangioma	1	6.5			
Bursa	1	8.3			

*Grade not classified due to small size of biopsy.
†Multiple nodules over an area of more than 5 cm diameter.
I = low grade; II = intermediate grade and III = high grade.

MATERIALS AND METHODS

Patients

Twenty-two patients (13 men, 9 women; aged 18–82 yr; mean age 50 yr) were included in the study. A malignant soft-tissue tumor was considered to be present in all patients based on clinical findings. Patients with recurrent soft-tissue sarcoma were not included in this analysis. Informed consent was obtained from each patient. One patient suffered from diabetes mellitus. Twenty lesions were localized in a lower extremity, two on an upper extremity. All relevant patient data are presented in Table 1.

Median lesion size was 7.0 cm (range 2.4–31.0 cm). All lesions were biopsied for pathologic evaluation. Eighteen patients had a soft-tissue sarcoma and four had a benign lesion. Malignant tumors were classified according to tumor type and were assigned a malignancy grade in a standard fashion (*2,3*).

PET

Fluorine-18 was produced using the $^{18}O(p, n)^{18}F$ reaction on enriched water. Synthesis of FDG was performed using the technique as described by Hamacher (*4*). The radiochemical purity was more than 98%. Images were acquired on a PET camera whose performance characteristics have been previously described (*5*). The camera acquires 31 contiguous slices simultaneously over a total axial length of 10.8 cm. The spatial resolution in the transaxial field of view in the stationary mode is 6.1 mm FWHM.

Patients fasted for 6 hr prior to the PET study. A 20-gauge needle was inserted into the radial artery at the wrist while the patient was under local anesthesia. An intravenous canula was inserted in the contralateral arm in the cephalic vein for the FDG injection. Images were acquired with the patient positioned supine and with the tumor in the field of view.

Following acquisition of an attenuation scan for which a ^{68}Ge ^{68}Ga source was used, FDG was administered for 1 min. The average dose was 370 MBq (10 mCi), range 185–407 MBq (5–11 mCi). Scanning was started at the time of injection following a dynamic protocol (five 1-min, five 2-min, five 3-min, two 5-min and two 10-min scans for a total scan time of 60 min). Simultaneously, 2-ml blood samples were taken from the arterial canula (time points: 0.5, 1, 1.5, 2, 2.5, 3, 3.5, 4, 4.5, 5, 10, 15, 25, 35, 45 and 55 min postinjection). The blood samples were centrifuged and plasma activity was assessed using a well counter that was cross-calibrated with the positron camera. The entire procedure took approximately 90 min. In some patients, additional whole-body images were obtained after dynamic imaging had been completed.

Data Analysis

The PET images were interpreted independently by two experienced physicians. Differences were resolved by consensus. The RMR_{gl} values were calculated using the following technique. A lesion was first defined in all relevant tomographic planes of the study. Each lesion was outlined automatically with a threshold technique that defines its contours at a manually chosen percentage of the maximum number of counts per pixel. The level of the threshold was chosen with the purpose of matching the region of interest size with the tumor size as outlined by MRI or CT. For each patient, a fixed percentage (median 40, range 30–60) was used in all planes. All pixels above the threshold were used for the calculation. An average time-activity curve as well as the total volume of the lesion were obtained. Microscopic areas of necrosis that are of importance in determining the malignancy grade were included in these calculations because of partial volume effects. Larger areas of necrosis were excluded.

The average RMR_{gl} (μmole/100 g/min) was calculated by combining the time-activity data with the plasma input data and using Patlak analysis with a lumped constant of 0.42 (*6,7*). In patients with negative scans, the RMR_{gl} was calculated for the region where the lesion was known to be. It was not possible to calculate RMR_{gl} in three patients due to technical causes.

The SUVs for the lesions were calculated using the equation:

$$\frac{A_{tumor}/V_{tumor}}{ID/bw},$$

where A_{tumor} = activity in the tumor, V_{tumor} = tumor volume, ID = injected dose and bw = body weight.

Statistical analysis included Kruskal-Wallis analysis of variance (ANOVA) for nonparametric tests to assess significant differences in RMR_{gl} and SUVs between groups. Post-hoc analysis consisted of Mann-Whitney U-tests. In addition, a correlation between the RMR_{gl} and the SUV was calculated. Probability values of less than 0.05 were significant.

TABLE 2
Diagnosis, Tumor Malignancy Grade, Visual Scan Assessment, RMR_{gl} (μmole/100 g/min) and SUV

Patient no.	Diagnosis	Grade	Scan	RMR_{gl}	SUV
1	Malignant fibrous histiocytoma	+	+	36.3	6.6
2	Malignant fibrous histiocytoma	I	+	2.9	6.3
3	Liposarcoma	I	+	4.3	1.4
4	Malignant fibrous histiocytoma	I	+	4.8	1.1
5	Liposarcoma (dedifferentiated)	II	+	*	*
6	Extraskeletal chondrosarcoma	II	+	3.9	0.8
7	Liposarcoma	II	+	9.5	2.5
8	Liposarcoma	II	+	12.5	2.5
9	Fibrosarcoma	III	+	*	*
10	Synovial sarcoma	III	+	12.5	2.4
11	Sarcoma, not otherwise classified	III	+	19.0	2.6
12	Synoviosarcoma	III	+	18.0	3.1
13	Malignant fibrous histiocytoma	III	+	13.0	3.2
14	Malignant fibrous histiocytoma	III	+	*	*
15	Neuroepithelioma	III	+	33.2	1.4
16	Rhabdomyosarcoma	III	+	36.7	6.1
17	Liposarcoma	III	+	41.8	2.9
18	Malignant fibrous histiocytoma	III	+	24.2	4.7
19	Lymphangioma		−	5.2	1.5
20	Myxoma		−	2.9	0.7
21	Bursa		±	10.6	1.9
22	Ganglion		+	5.4	1.3

*Not calculated due to technical failure.
†No classification possible due to limited amount of tissue.
I = low malignancy grade; II = intermediate grade; II = high grade.

RESULTS

All soft-tissue sarcomas were easily detected on the PET images (Table 2) and a typical example is presented in Figure 1. Soft-tissue sarcomas are often inhomogeneous on pathologic examination. Necrosis and hemorrhage can be interspersed in areas with viable neoplastic cells. This variable texture of a sarcoma is reflected by inhomogeneous FDG uptake (Fig. 2). One of the four benign lesions was visualized on the scans, one scan was equivocal and two were negative.

The RMR_{gl} and SUV of each patient are presented in Table 2. The median RMR_{gl} for all malignant tumors was 13.0 μmole/100 g/min (range 2.9–41.8 μmole/100 g/min). The RMR_{gl} range for the benign lesions was 2.9–10.6 μmole/100 g/min. A significant difference in RMR_{gl} was found between the various malignancy grades when the benign lesions were included, as well as when the benign lesions were excluded (Kruskal-Wallis ANOVA). Such a significant difference was not found for the SUV ($p = 0.11$ and 0.29, respectively).

Post-hoc analysis proved the difference in RMR_{gl} to be related to marked glucose uptake in high-grade sarcomas. A significant difference was found between high-grade and low-grade sarcomas and also between intermediate grade sarcomas and benign lesions. Therefore, benign lesions could be discerned by a lower RMR_{gl} from tumors with a high malignancy grade. Some overlap in RMR_{gl} was present in between benign and intermediate grade lesions. Benign lesions could not be distinguished from low-grade lesions ($p > 0.05$). A significant difference in SUV was only found between high-grade sarcomas and benign lesions.

FIGURE 1. Patient with an intermediate grade myxoid liposarcoma of the left thigh, (dimensions 11 × 5 × 5 cm). The anterior view of the whole-body PET study shows increased FDG uptake in the tumor.

DISCUSSION

Tumor Detection

This study explores PET's ability to analyze tissue biology in vivo and confirms the tumor imaging potential of FDG. High uptake of FDG in various histologic types of soft-tissue sarcoma is demonstrated. This resulted in a sensitivity of 100% in the visualization of these lesions. Small and large tumors were depicted equally well. Our results confirm the excellent sensitivity reported by other investigators (*8–10*). Only one false-negative FDG scan in a patient with soft tissue sarcoma has been described (*11*).

Soft-tissue sarcomas are often inhomogeneous. Different parts within a tumor may have different malignancy grades. Stroma, necrosis, hemorrhage and edema may be found within a tumor. The PET study depicted in Figure 2 shows that FDG uptake can be variable within a tumor. Thus, FDG-PET may

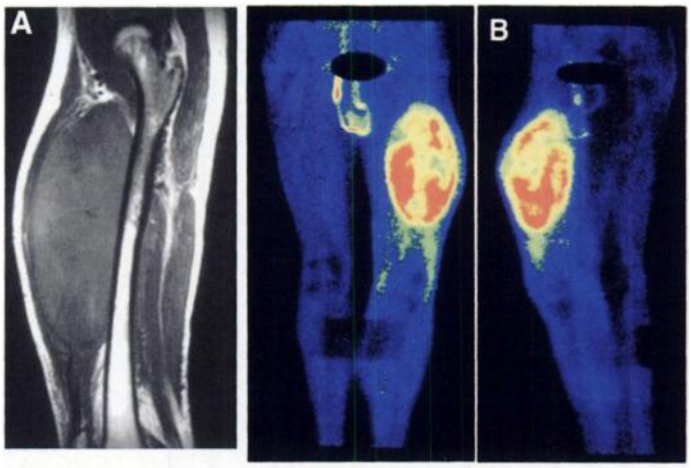

FIGURE 2. (A) MRI of a patient with a large (8.0 × 12.5 cm) high-grade fibrosarcoma of the left thigh. (B) Whole-body PET study with inhomogeneous FDG uptake in the tumor, anterior view (left) and lateral view (right).

provide important information about metabolic activity and may be useful in guiding biopsy of patients with large lesions (*10,12*).

The use of FDG is based on the observations by Warburg that malignant cells accumulate more glucose than normal cells due to a predominantly glycolytic catabolism instead of a citric acid cycle catabolism (*13*). Tumor cells have an increased demand for glucose because glycolysis yields considerably less adenosine triphosphate from the same amount of glucose. More recent studies have shown that malignant tumor cells have increased levels of glucose transporters on the cell membrane. In using immunohistochemistry techniques, Brown and Wahl demonstrated an increased expression of Glut-1 glucose transporter in breast cancer (*14*). Others investigators have indicated that increased expression of Glut-1 protein, of the corresponding messenger RNA and increased uptake of glucose and FDG are associated with transformation to malignancy (*15,16*). It is tempting to speculate that increased expression of the glucose transporter is a reaction to the less efficient adenosine triphosphate synthesis to meet the increased demand for energy.

Malignancy Grade

The RMR_{gl} calculation from FDG-PET studies is well validated for the brain (*17*) and myocardium (*18*). There is, however, no generally applicable kinetic model for tumors. Our calculations of glucose metabolism in sarcoma are based on several assumptions. First, hexokinase and glucose-6-phosphatase activity in sarcoma and brain are equal. Second, there is no back diffusion of FDG-6-phosphate through the cell membrane. These extrapolations allowed us to use the lumped constant of 0.42 for our calculations. Whether these assumptions are justified is unclear at this time. A study is currently underway to establish whether our approach can be validated. It is known that the lumped constants of gliomas and normal brain are different (*19–21*). It is likely that malignant tumors and normal brain tissue also have a different lumped constant. It is also reasonable to assume that the lumped constant is different in various types of tumors. The way to find this out is to repeat the original experiments of Sokoloff and Phelps, for instance in human cell lines implanted in rats (*22*).

This study indicates a correlation between tumor malignancy grade and the level of RMR_{gl}. Interestingly, this correlation appears to hold true for various histologic sarcoma types, in that soft-tissue sarcomas can arise in widely diverging tissues. Other investigators have speculated that such a correlation may exist (*8,9*). A similar correlation has been found in brain tumors (*23*) and has been suggested in non-Hodgkin's lymphoma (*24*).

As an alternative to calculating (absolute) glucose consumption, many clinicians use SUV. This is a relative measure of uptake activity in a tissue of interest in comparison to the whole-body distribution. The distinct advantage of using the SUV is its ease, thereby obviating the need for arterial blood sampling. On the other hand, no absolute metabolic values are obtained in this fashion. In our series of patients, the SUV did not distinguish between high-grade and low-grade malignancies, whereas the RMR_{gl} did. Thus, calculating RMR_{gl} is preferable when determination of malignancy grade is desired.

The values of RMR_{gl} and SUV are influenced by the resolution of the imaging system (partial volume effect). Modern cameras have a resolution of 0.6 cm FWHM or less; therefore, this problem affects imaging of small tumors. Since the smallest tumor in our series was 2.4 cm in diameter, we do not believe that results were influenced by this phenomenon. The possibility, however, of undergrading smaller lesions should be considered.

Malignancy grade is an important indicator of the stage of a soft-tissue sarcoma and is one of the parameters that directs the selection of a treatment regimen. Unfortunately, malignancy grade is often difficult to establish. Competent pathologists often disagree on this matter. There is only a 75% concordance rate in assigning such a grade (*2*). Therefore, the current finding of a correlation between glucose consumption and malignancy grade is important. A noninvasive diagnostic technique as an aid to establishing tumor grade may be of value in the treatment of patients with soft-tissue sarcoma. The fact that PET is performed on tumors in vivo offers a particularly interesting potential.

Benign Lesions

Increased uptake in one of four patients with a benign lesion and equivocal uptake in another are disappointing findings. FDG does not appear to be informative in the differential diagnosis of a soft-tissue mass, except to depict a high-grade malignant lesion. Uptake of FDG in benign soft-tissue masses has also been seen by other investigators (*10,25*). Despite this increased uptake, these investigators were able to differentiate between benign and malignant soft-tissue tumors using FDG and SUVs (*9,10*). In view of those findings, our inability to confirm this uptake using RMR_{gl}, should be viewed cautiously. The limited number of patients with a benign lesion in our study adds to this restraint. Moreover, other radiopharmaceuticals may be worth investigating.

CONCLUSION

Our results indicate that FDG-PET can be of value in selected patients with soft-tissue sarcoma. FDG-PET is not, however, ready to assume a position in the routine clinical evaluation of these patients. In patients with large lesions, PET may indicate a good site for biopsy. The information that PET provides about malignancy grade of the whole tumor may be important when preoperative chemotherapy or radiotherapy is contemplated.

Our findings reinforce the basis for subsequent clinical PET research for these types of tumors. A future study may explore FDG-PET in the screening for metastases. Can "whole body" scanning detect blood borne metastases not visible with conventional radiographic techniques? That soft-tissue sarcomas usually disseminate to the lungs and that FDG accumulation in

the lungs is low suggest the potential clinical value of PET for tumor staging. Another clinical application of FDG-PET may be early detection of locally recurrent tumors. After surgery and radiotherapy, recurrent lesions are usually difficult to detect in the early phase. Physical examination and Roentgen techniques are hampered by scar tissue and distortion of the normal tissue planes, disadvantages that PET does not have. Future PET investigations should also be aimed at the application of other radiopharmaceuticals such as labeled amino acids, DNA substrates and chemotherapeutic drugs. Evaluation of radiotherapeutic and chemotherapeutic results for soft-tissue sarcoma also seem attractive fields for future PET studies.

REFERENCES

1. Strauss LG, Conti PS. The applications of PET in clinical oncology. *J Nucl Med* 1991;32:623–648.
2. Coindre JM, Trojani M, Contesso G, et al. Reproducibility of a histopathologic grading system for adult soft-tissue sarcoma. *Cancer* 1986;58:306–309.
3. Enzinger FM, Weiss SW. *Soft-tissue tumors*. St. Louis: CV Mosby; 1988.
4. Hamacher K, Coenen HH, Stocklin G. Efficient stereospecific synthesis of no-carrier added 2-[^{18}F]-fluoro-2-deoxy-D-glucose using aminopolyether supported nucleophilic substitution. *J Nucl Med* 1986;27:235–238.
5. Paans AMJ, Tilkema SP, Pruim J, et al. Performance parameters of the Siemens 951 ECAT positron camera with its new computer configuration [Abstract]. *Eur J Nucl Med* 1991;18:603.
6. Patlak CS, Blasberg RG, Fenstermacher JD. Graphical evaluation of blood-to-brain transfer constants from multiple-time uptake data. *J Cereb Blood Flow Metab* 1983;3:1–7.
7. Patlak CS, Blasberg RG. Graphical evaluation of blood-to-brain transfer constants from multiple-time uptake data. Generalizations. *J Cereb Blood Flow Metab* 1985;5:584–590.
8. Kern KA, Brunetti A, Norton JA, et al. Metabolic imaging of human extremity musculoskeletal tumors by PET. *J Nucl Med* 1988;29:181–186.
9. Adler LP, Blair HF, Makley JT, et al. Noninvasive grading of musculoskeletal tumors using PET. *J Nucl Med* 1991;32:1508–1512.
10. Griffeth LK, Dehdashti F, McGuire AH, et al. PET evaluation of soft-tissue masses with fluorine-18 fluoro-2-deoxy-D-glucose. *Radiology* 1992;182:185–194.
11. Kubota K, Matsuzawa T, Fujiwara T, et al. Differential diagnosis of lung tumor with positron emission tomography: a prospective study. *J Nucl Med* 1990;31:1927–1933.
12. Adler LP, Blair HF, Williams RP, et al. Grading liposarcomas with PET using [^{18}F]FDG. *J Comput Assist Tomogr* 1990;14:960–962.
13. Warburg O. On the origin of cancer cells. *Science* 1956;123:309–314.
14. Brown RS, Wahl RL. Overexpression of Glut-1 glucose transporter in human breast cancer. *Cancer* 1993;72:2979–2985.
15. Flier JS, Mueckler MM, Usher P, Lodish HF. Elevated levels of glucose transport and transporter messenger RNA are induced by ras or src oncogenes. *Science* 1987;235: 1492–1495.
16. Su TS, Tsai TF, Chi CW, Han SH, Chou CK. Elevation of facilitated glucose-transporter messenger RNA in human hepatocellular carcinoma. *Hepatology* 1990;11:118–122.
17. Sokoloff L, Reivich M, Kennedy C, et al. The [^{14}C]deoxyglucose method for the measurement of local cerebral glucose utilization: theory, procedure and normal values in the conscious and anesthetized albino rat. *J Neurochem* 1977;28:897–916.
18. Marshall RC, Huang SC, Nash WW, Phelps ME. Assessment of the [^{18}F]fluorodeoxyglucose kinetic model in calculations of myocardial glucose metabolism during ischemia. *J Nucl Med* 1983;24:1060–1064.
19. Graham JF, Cummins CJ, Smith BH, Kornblith PL. Regulation of hexokinase in cultured gliomas. *Neurosurg* 1985;17:537–542.
20. Kapoor R, Spence AM, Muzi M, Graham MM, Abbott GL, Krohn KA. Determination of the deoxyglucose and glucose phosphorylation ratio and the lumped constant in rat brain and a transplantable rat glioma. *J Neurochem* 1989;53:37–44.
21. Spence AM, Graham MM, Muzi M, et al. Deoxyglucose lumped constant estimated in a transplanted rat astrocytic glioma by the hexose utilization index. *J Cereb Blood Flow Metab* 1990;10:190–198.
22. Sokoloff L. Cerebral circulation, energy metabolism and protein synthesis: general characteristics and principles of measurement. In: Phelps ME, Mazziotta JC, Schelbert HR, eds. *Positron emission tomography and autoradiography. Principles and applications for the brain and the heart*. New York: Raven Press; 1986:1–72.
23. Di Chiro G, DeLaPaz RL, Brooks RA, et al. Glucose utilization of cerebral gliomas measured by ^{18}F-fluorodeoxyglucose and positron emission tomography. *Neurology* 1982;32:1323–1329.
24. Leskinen-Kallio S, Ruotsalainen U, Nagren K, Teras M, Joensuu H. Uptake of carbon-11-methionine and fluorodeoxyglucose in non-Hodgkin's lymphoma: a PET study. *J Nucl Med* 1991;32:1211–1218.
25. Adler LP, Blair HF, Makley JT, Pathria MN, Miraldi F. Comparison of PET with CT, MRI and conventional scintigraphy in a benign and in a malignant soft-tissue tumor. *Orthopedics* 1992;14:891–895.

Dynamic Cholescintigraphy: Induction and Description of Gallbladder Emptying

Dorte B. Toftdahl, Liselotte Højgaard and Kjeld Winkler

Departments of Medical Gastroenterology and Clinical Physiology/Nuclear Medicine, Hvidovre Hospital, University of Copenhagen, Denmark

The main purposes of this study were to investigate the best parameter for describing gallbladder emptying and whether gallbladder bile emptying should be induced with a bolus injection or continuous infusion of cholecystokinin-octapeptide (CCK-8). **Methods:** Gallbladder emptying was measured by dynamic cholescintigraphy. Twelve healthy subjects and six patients with gallstones were examined twice with CCK-8 infusion cholescintigraphy, 0.3 ng CCK-8 kg per min for 60 min under identical circumstances. Another six healthy subjects randomly received bolus injection (0.04 μg/kg) and infusion of CCK-8 (0.3 ng/kg per min for 60 min), respectively, during cholescintigraphy on two separate occasions. The choice of bolus dose was based on recommendations from the CCK-8 manufacturer. The infusion dose was chosen to produce plasma CCK concentrations similar to postprandial plasma CCK levels. **Results:** A parameter of gallbladder emptying, mean ejection fraction (EF), was defined as 100% minus the area under the time-activity curve normalized to 100% and divided by the time interval from maximum to minimum counts per minute. This parameter proved superior to the well known parameters, EF_{max} and EF_{30}, in regard to reproducibility in healthy subjects. The slope of the regression line for the mean EF was 0.998 and the intercept value approximately 0% ($p = 0.0001$). The mean coefficient of variation was 4%. Apart from a higher mean coefficient of variation, similar reproducibility results were seen in the six patients. The measurements of EF_{30} in healthy subjects scattered more widely around the mean compared to the mean EF and EF_{max}, which indicates poorer ability to separate normal from abnormal gallbladder emptying. Intravenous bolus injection of CCK-8 resulted in incomplete gallbladder emptying with a mean EF value of 16% (s.d. 9%; range 7%–32%) compared to 49% (s.d. 7%; range 37%–57%) following CCK-8 infusion ($p = 0.004$). Abdominal discomfort was observed in all subjects after administration of the bolus injection, whereas no complaints were reported during infusion. **Conclusion:** Mean EF is the best parameter for describing gallbladder emptying. Moreover, slow infusion of a physiological dose of CCK-8 is preferable to induce gallbladder emptying because it results in more complete emptying and has no side effects.

Key Words: dynamic cholescintigraphy; gallbladder emptying; cholecystokinin-octapeptide

J Nucl Med 1996; 37:261–266

Received Dec. 19, 1995; revision accepted Jul. 30, 1995.

For correspondence or reprints contact: Dorte B. Toftdahl, MD, Skraenten 3, Gadevang, DK-3400 Hilleroed, Denmark.